

COMPARISON OF TOTAL SOLAR IRRADIANCE WITH NASA/NATIONAL SOLAR OBSERVATORY SPECTROMAGNETOGRAPH DATA IN SOLAR CYCLES 22 AND 23

HARRISON P. JONES

NASA Goddard Space Flight Center, Laboratory for Astronomy and Solar Physics, Southwest Solar Station, c/o National Solar Observatory,¹
P.O. Box 26732, Tucson, AZ 85726; hjones@noao.edu

DETRICK D. BRANSTON

National Solar Observatory, P.O. Box 26732, Tucson, AZ 86726; dbranston@noao.edu

PATRICIA B. JONES

University of Arizona, Center for Computing and Information Technology, Tucson, AZ 85721; pjones@jemez.rc.arizona.edu

AND

MIRUNA D. POPESCU²

Astronomical Institute of the Romanian Academy, RO-75212 Bucharest 28, Romania; mdp@star.arm.ac.uk

Received 2002 December 9; accepted 2003 January 30

ABSTRACT

NASA/National Solar Observatory Spectromagnetograph (SPM) data are compared with spacecraft measurements of total solar irradiance (TSI) variations for 8 yr beginning with the declining phase of solar cycle 22 and extending into the maximum of cycle 23. Previously reported conclusions based on a similar comparison for a shorter time period appear to be robust: three factors (sunspots, strong unipolar regions, and strong mixed-polarity regions) describe most of the variation in the SPM record, but only the first two are associated with TSI. Additionally, the residuals of a linear multiple regression of TSI against SPM observations over the entire 8 yr period show an unexplained, increasing, linear time variation with a rate of about $0.05 \text{ W m}^{-2} \text{ yr}^{-1}$. Separate regressions for the periods before and after 1996 January 1 show no unexplained trends but differ substantially in regression parameters. This behavior may reflect a solar source of TSI variations beyond sunspots or uncompensated nonsolar effects in one or both of the TSI and SPM data sets.

Subject headings: Sun: activity — Sun: magnetic fields

1. INTRODUCTION

Accurate understanding of global solar variability is of clear astrophysical interest and is also vital to distinguish natural from anthropogenic causes of long-term changes in terrestrial climate. Daily averages of total solar irradiance (TSI) observations from several spacecraft radiometers over the past two decades show clear rotational and solar-cycle variations (Pap & Fröhlich 1999; Fröhlich & Lean 1998; Fröhlich 2000). The modeling of this variability through comparison of the spacecraft measurements with spatially resolved solar observations from both ground- and space-based instruments is highly refined (Chapman, Cookson, & Dobias 1996; Foukal & Lean 1988; Fligge, Solanki, & Unruh 2000; Preminger, Walton, & Chapman 2002). Two classes of solar features, dark sunspots and bright faculae, account for about 90% of the TSI variance. Although it is not yet clear whether the remaining discrepancies are observational or require additional sources of irradiance variability, the simple observation (de Toma et al. 2001) that TSI at the current solar maximum is very similar to the previous maximum while photospheric indicators of solar activity are lower in cycle 23 than in cycle 22 hints that more than solar activity is involved. This paper presents more detailed evidence to support this idea.

¹ The National Solar Observatory is operated by the Association of Universities for Research in Astronomy under cooperative agreement with the National Science Foundation.

² Also at Armagh Observatory, College Hill, Armagh BT61 9DG, Northern Ireland.

2. OBSERVATIONS

The results discussed here are based on two data sets. One of these is the set of daily full-disk magnetograms from the NASA/National Solar Observatory (NSO) Spectromagnetograph (SPM) that consist of strictly cospatial and cotemporal full-disk images of line-of-sight (LOS) magnetic flux, LOS velocity, continuum intensity, equivalent width, and central line depth derived from long-slit spectral polarimetry of the Fe I 868.8 nm line. The observations have $1''.14 \times 1''.14$ spatial pixels, approximately 42 mÅ spectral pixels, and a magnetic noise level of about 5 G. Data for 2194 days from 1992 November 21 to 2000 September 30 are reduced and analyzed here. A more complete description of the instrument and data is given by Jones et al. (2000, hereafter JBJW).

The other data set is the composite measure of TSI compiled from various spacecraft from 1979 through the present by Fröhlich & Lean (1998) and Fröhlich (2000), who describe the individual observations and the techniques used to combine them into a single data stream. For this study we use version 23 of the composite measure of TSI from the Physikalisch-Meteorologisches Observatorium Davos World Radiation Center, Davos, Switzerland, which includes unpublished data from the Variability of Solar Irradiance and Gravity (VIRGO) experiment on the cooperative ESA/NASA *Solar and Heliospheric Observatory (SOHO)*. Data from both the composite TSI and the SPM were available for 2123 days during the interval from 1992 November 21 to 2000 September 30.

3. ANALYSIS

No adjustments or filtering were performed on the composite TSI data other than to select days for which both SPM and TSI observations were available. The reduction of the SPM data was carried out exactly as described in JBJW. Low-order, least-squares spatial fits of the daily data were applied to remove spurious instrumental and telluric effects as well as unwanted solar center-to-limb variations. Daily multidimensional histograms were computed from the five input images, and solar “features” were defined by restricted domains in the histogram variable space as described by JBJW. Area and contrast measures of each of the features were computed from the histograms as described below and in more detail in JBJW. Factor analysis using principal component extraction revealed the most important linear combinations of the original feature measures for explaining the variability of the SPM data, and a multiple regression of the TSI observations as a function of these factors was performed. This analysis procedure was meant to be exploratory, allowing efficient multiple passes through our data set to learn what important features in the SPM data are related to TSI without building in strong prejudices. We did indeed experiment with domain limits different from JBJW for the various features, but this did not affect the substantive results of our study.

Specifically, we considered nine categories of solar features: weak field, sunspot penumbra, sunspot umbra, bright (and dark) strong-field unipolar features in the central portion of the disk, bright (and dark) strong-field mixed-polarity features in the central portion of the disk, and bright (and dark) strong-field features near the solar limb. Bright and dark features are distinguished by continuum (not bolometric) intensity contrast at 868.8 nm with reference to the fitted limb-darkening curve. The defining parameter domains for these features both as used by JBJW and an alternative classification are given in Table 1, where B is in gauss, i and q are intensity and equivalent width contrasts with respect to local center-to-limb variation, and μ is the

cosine of the heliocentric angle from disk center. “Unipolarity,” u , is defined here as the fraction of flux of one sign in a roughly supergranular area surrounding a given point on the disk and is divided into four bins in the multidimensional histograms. The revised feature classification is based on that used by Jones (1998) to search for possible thermodynamic differences between unipolar and mixed-polarity features. The revised and original classifications differ mostly in the division of unipolar and mixed-polarity features. Roughly speaking, strong unipolar regions correspond to active regions, including some of the enhanced network that trails from older active regions, while strong mixed-polarity regions correspond to magnetic network outside of active regions. The revised feature definitions count more enhanced network as unipolar.

An important pedagogic distinction between the two histogram feature classifications is that the original definitions contain some overlap between features. Pixels in the overlapping domains are counted more than once in the subsequent analysis procedure, which influences the correlations between variables and resulting factor structure. Although this effect has proved to be small, the revised feature definitions contain no overlapping regions and are used for this paper. Note as well that neither set of classifications are formally complete. Practically, however, the neglected regions of the histograms are sparse, and the total number of pixels in the included domains equals the actual total number of pixels within the accuracy of the interpolation techniques that are used to extract this information from the variably binned histograms (see JBJW).

As in JBJW, for each histogram feature we compute the fractional area (number of pixels relative to the total number of pixels) and differential contrasts in intensity, equivalent width, and central line depth relative to the weak-field pixels in the same domains of u and μ . As basis sets for subsequent factor analysis, we use two different subsets of these quantities. In both cases, we include fractional area and differential contrasts for each of the feature classes except weak fields, where the differential contrasts are zero by

TABLE 1
HISTOGRAM FEATURE DOMAINS

Class	$ B $ (G)	i	q	μ	u
Weak	[0, 8]	All	All	[0, 1]	[0, 1]
Penumbra	(128, 768]	[-0.3, 0.0]	>0.05	[0, 1]	[0, 1]
Umbra	>128	<-0.3	All	[0, 1]	[0, 1]
Disk center (original):					
Bright mixed polarity	(8, 256]	>0.0	All	[0.5, 1.0]	<0.75
Bright unipolar.....	(8, 256]	>0.0	All	[0.5, 1.0]	>0.75
Dark mixed polarity	(8, 256]	<0.0	All	[0.5, 1.0]	<0.75
Dark unipolar	(8, 256]	<0.0	All	[0.5, 1.0]	>0.75
Limb (original):					
Bright.....	(8, 256]	≥ 0.0	All	[0, 0.5]	[0, 1]
Dark	(8, 256]	<0.0	All	[0, 0.5]	[0, 1]
Disk center (revised):					
Bright mixed polarity	(8, 256]	[0.0, 0.1]	[-0.1, 0.05]	[0.5, 1.0]	<0.5
Bright unipolar.....	(8, 256]	[0.0, 0.1]	[-0.1, 0.05]	[0.5, 1.0]	>0.5
Dark mixed polarity	(8, 256]	[-0.1, 0.0]	[-0.1, 0.05]	[0.5, 1.0]	<0.5
Dark unipolar	(8, 256]	[-0.1, 0.0]	[-0.1, 0.05]	[0.5, 1.0]	>0.5
Limb (revised):					
Bright.....	(8, 256]	≥ 0.0	All	[0, 0.5]	[0, 1]
Dark	(8, 256]	[-0.3, 0.0]	<0.05	[0, 0.5]	[0, 1]

definition. In the “original” basis set used by JBJW, we also include weak-field fractional areas for the whole disk, disk-center unipolar and mixed-polarity regions, and limb. In the “new” set, we include instead the weak-field fractional area and contrasts with respect to limb darkening for intensity, equivalent width, and line depth for the whole disk. Our substantive conclusions do not depend on which feature definition or basis set is used.

Altogether, 36 variables are computed for either basis set. Factor analysis (see, for example, Harman 1976), which models the observed variables as a linear combination of unknown “common” factors plus unique variability (including noise), is used to reduce the dimensionality of the original basis by accounting for cross-correlations. Rather than iteratively solving the complete factor analysis model, we fix the unique variability at zero and identify the common factors as the principal components (eigenvectors) of the correlation matrix, select from inspection of the eigenvalue “scree” plot the factors with the six largest eigenvalues, and perform an orthogonal “varimax” rotation of these to maximize the column variance of the factor loading matrix while maintaining zero cross-correlation between factors. The rotated factors, which are linear combinations of the original variable set, account for most of the variance in the SPM data and have relatively unambiguous interpretations in terms of solar features. A more detailed description of this process is given in JBJW. Finally, we perform a multiple regression with TSI as dependent and SPM factors as independent variables.

Since the work of JBJW, the accuracy of the algorithm for computing the weak-field reference contrasts for intensity, equivalent width, and line depth has been improved. In this paper, we report results from applying the improved algorithm to both the time period spanned by JBJW and that spanned by the complete data set. The factor loadings (correlations of the original variables with the factors) for the original and improved algorithms are highly correlated, and our conclusions would remain unchanged had we used the original algorithm. Although any combination of feature definitions and basis sets that we tried leads to the same conclusions, computations using the “new” basis variables extracted for the “revised” features show, by a small margin, the best combination of clear interpretability of the factor loadings and continuation of the factor structure over the entire time period and will be displayed in this paper.

4. RESULTS

4.1. Factor Analysis

Figure 1 shows the fraction of explained variance for both the unrotated and rotated factors over the entire time period of the SPM observations. The six retained factors explain about 84% of the SPM variance, while the dominant three factors alone account for about 69%. We assume that the remaining 30 components, whose eigenvalues slowly decay to zero and which both individually and cumulatively account for a small fraction of the SPM variance, are primarily indicative of noise in the data. Note that only the first three factors show significant changes in explained variance as a result of the orthogonal rotation.

Figure 2 shows the rotated factor loadings (i.e., the correlations of each factor with each of the original basis variables) in bar graph form for the entire observing period (1991

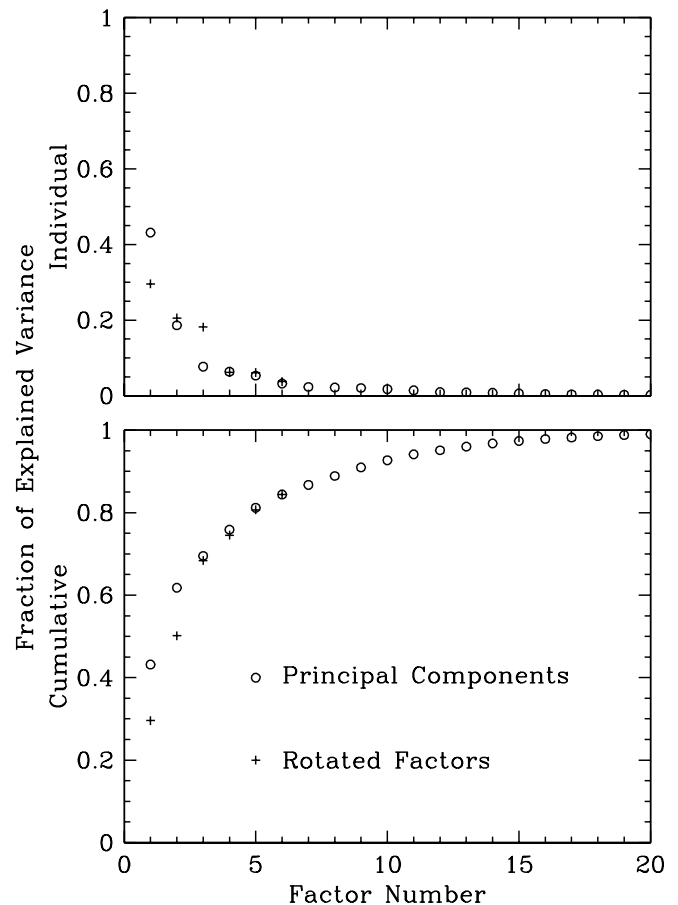


FIG. 1.—Proportion of explained variance as a function of factor number. The upper panel shows contributions for each factor individually, and the lower panel shows cumulative contribution. Open circles show the non-rotated factors (principal components), while plus signs denote the six rotated factors.

November 21–2000 September 30). Factors are numbered in decreasing order of explained variance. Over this period, the most important factor, factor 1, is highly correlated with fractional area and differential contrasts of intensity, equivalent width, and line depth for both bright and dark unipolar, disk-center features and bright limb features (with the exception of equivalent width for dark disk-center features) and fractional area of dark limb features and weak-field structures. This loading pattern represents spatial structures associated with active regions outside of sunspots together with enhanced unipolar network and at least roughly corresponds to faculae in the standard model of TSI variations. Factor 2 is associated with area and contrasts in sunspots, while factor 3 depends on areas and contrasts for both bright and dark mixed-polarity, disk-center features (again with the exception of equivalent width for dark structures). One consequence of our revised feature definition is the cleaner separation of unipolar and mixed-polarity regions in factors 1 and 3 than the original classification of JBJW while factor 1, representing primarily faculae, shows stronger correlation with sunspots. As will be shown more quantitatively below, the dominant three factors closely correspond to the factor structure described by JBJW for the limited time period.

Although we do not yet understand how the loading patterns for the three minor factors relate to conventionally recognized solar features, they consistently appear with the

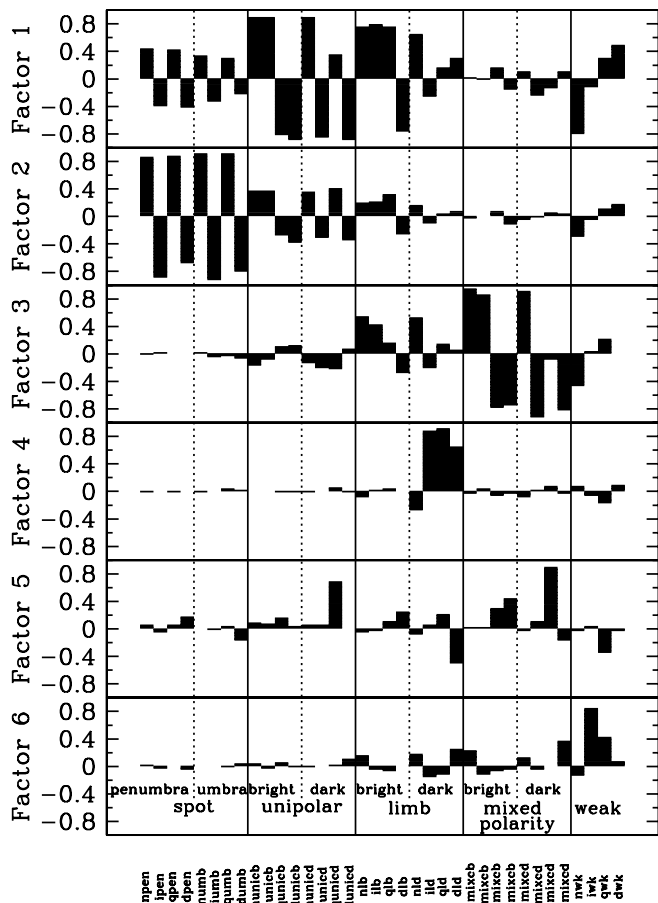


Fig. 2.—Bar graph of the correlation coefficients between the rotated factors and original variables (factor loadings) for the entire SPM observation period. The x -axis is labeled by original variable: i , q , and d denote contrasts of intensity, equivalent width, and central line depth; n denotes fractional number of pixels (area); “pen” refers to sunspot penumbra, “umb” to umbra, “unicb(d)” to unipolar disk-center bright (dark) pixels, “mixcb(d)” to mixed-polarity disk-center bright (dark) pixels, “lb(d)” to limb-bright (dark) pixels, and “wk” to weak-field pixels.

improved analysis algorithm, new basis variable set, and revised feature definitions regardless of sampling period. Differential contrasts of intensity, equivalent width, and line depth in dark limb features are related to factor 4; factor 5 is primarily correlated with differential contrast of equivalent width for dark disk-center structures, regardless of unipolarity; and factor 6 is associated with contrasts of intensity (primarily) and equivalent width (secondarily) of weak magnetic elements.

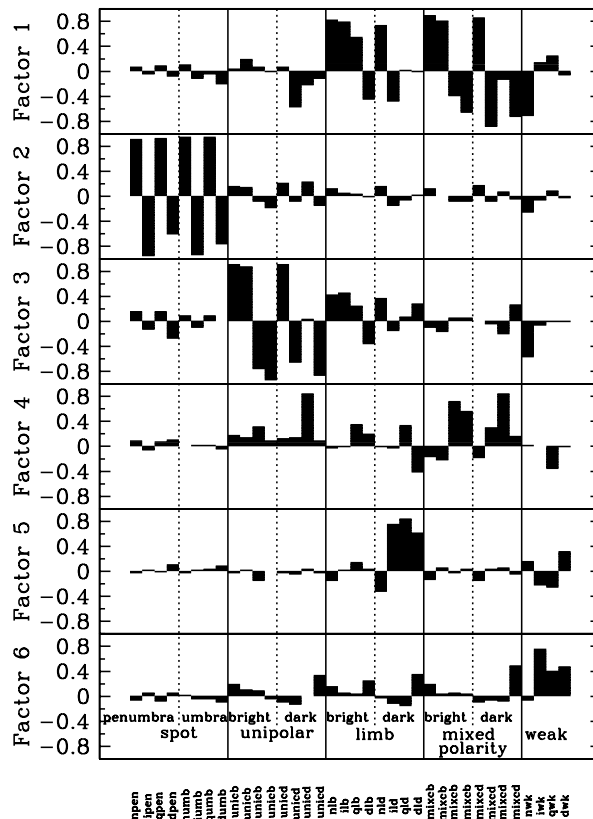


Fig. 3.—Factor loadings for the initial SPM period treated by JBJW in the format of Fig. 2.

Figure 3 shows the rotated factor loadings for the original period treated by JBJW (1991 November 21–1994 March 30). Except for minor interchanges of order (factors 1 and 3 as well as 4 and 5), Figures 2 and 3 are visually very similar. The loading patterns are similar for all six of the retained factors and therefore are likely to reflect intrinsic properties rather than an accidental result of the sampling period. The different ordering over the two time periods reflects partly the varying importance of solar properties over different phases of the sunspot cycle and partly the near equality of explained variance among the relevant factors.

The stability of the factor patterns is more quantitatively verified in Table 2, which shows the correlation matrix of the two factor patterns. That is, letting $c_w(i, k)$ and $c_s(i, k)$ denote the correlations over time (factor loadings) of the i th factor with the k th basis variable for the whole and short time periods, respectively, the correlations over basis

TABLE 2
CORRELATION OF FACTOR PATTERNS

FACTORS FOR 1992 NOV 21–1994 MAR 30	FACTORS FOR 1992 NOV 21–2000 SEP 30					
	1	2	3	4	5	6
1.....	0.490	0.233	0.921	-0.207	-0.217	0.184
2.....	0.478	0.953	0.116	-0.091	0.073	0.040
3.....	0.920	0.507	0.019	-0.014	0.118	0.069
4.....	-0.055	0.085	-0.529	-0.034	0.890	-0.313
5.....	-0.043	-0.055	-0.170	0.955	-0.004	-0.402
6.....	0.058	-0.012	-0.011	-0.166	0.310	0.790

TABLE 3
MULTIPLE REGRESSIONS

FACTOR (SPM R^2)	1992 Nov 21–2000 SEP 30			1992 Nov 21–1995 DEC 31			1996 JAN 1–2000 SEP 30		
	Coefficient	Error	R^2	Coefficient	Error	R^2	Coefficient	Error	R^2
1 (0.30).....	0.346	0.004	0.681	0.205	0.007	0.482	0.376	0.004	0.765
2 (0.21).....	-0.111	0.004	0.071	-0.190	0.008	0.205	-0.134	0.004	0.100
3 (0.18).....	-0.012	0.004	0.001	-0.025	0.006	0.007	-0.040	0.004	0.007
4 (0.06).....	0.015	0.004	0.001	0.001	0.005	0.000	0.009	0.005	0.000
5 (0.06).....	0.028	0.004	0.005	0.009	0.006	0.001	0.043	0.004	0.009
6 (0.04).....	0.011	0.004	0.001	0.004	0.004	0.000	-0.032	0.007	0.002
Total (0.84).....			0.760			0.702			0.883
Trend.....	0.050	0.002	0.295	-0.006	0.006	0.001	0.006	0.003	0.003

variables,

$$C(i, j) = \sum_{k=1}^{36} [c_s(i, k) - \langle c_s(i) \rangle] \\ \times [c_w(j, k) - \langle c_w(j) \rangle] / [\sigma_s(i) \sigma_w(j)],$$

are shown in Table 2, where, for example, $\langle c_w(i) \rangle$ and $\sigma_w(i)$ denote the mean and standard deviation over basis variables of $c_w(i)$. Note that since c_w and c_s are different, $C(i, j)$ is not symmetric. Allowing for the difference in ordering noted above, the three major factor patterns have correlation coefficients of greater than 0.92 with each other and less than 0.51 with other factors. Similar but slightly weaker results apply to the three minor factors.

4.2. Multiple Regression

Table 3 shows the coefficients and their standard errors along with the fraction of explained variance (multiple R^2) for three regressions of composite TSI as a function of the six rotated factors. The first covers the total time period 1992 November 21–2000 September 30; the second and third regressions, following de Toma et al. (2001), are independent fits of the periods before and after 1996 January 1, a division date corresponding roughly to the minimum separating cycles 22 and 23 as well as the beginning of observations from the VIRGO radiometers. The bottom row of Table 3 shows the slopes in units of $\text{W m}^{-2} \text{yr}^{-1}$ of linear least-squares fits of the residuals (TSI–regression) for the three multiple regressions as a function of time together with the formal errors and fractions of the residual variances accounted for by the fits. The composite TSI (version 23) together with regression fits and residuals are plotted as functions of time in Figure 4.

For the total period, the six factors account for about 76% of the TSI variance, somewhat more than the similar analysis of JBJW but less than the best traditional analyses using the Photospheric Sunspot Index (PSI) and Photospheric Facular Index (PFI) (e.g., Chapman et al. 1996). Moreover, as in JBJW, unipolar regions (faculae) and sunspots account for almost all the explained variance, while strong-field mixed-polarity (quiet network) features, although accounting for a significant fraction of the SPM variance, are just barely correlated with TSI at the 3σ level and account for negligible amounts of TSI variance. For the declining phase of cycle 22, the second multiple regression accounts for noticeably less (70%) TSI variance, while the third multiple regression accounts for about 88% of the TSI variance in the growth and maximum phase of cycle 23. For

the latter two regressions, the major differences between TSI and SPM prediction occur on timescales of days to a rotational period, and the explained variance for cycle 23 is comparable to the best current fits obtained from other data. Although quiet network (factor 3) has coefficients in the latter two regressions that are statistically different from zero at better than 3σ , the feature accounts for less than 1% of the TSI variance in either case. Although the present analysis is in qualitative agreement with JBJW, the use of improved analysis algorithms and particularly revised feature definitions (see Table 1) changes details; unipolar regions and sunspots account for comparable amounts of

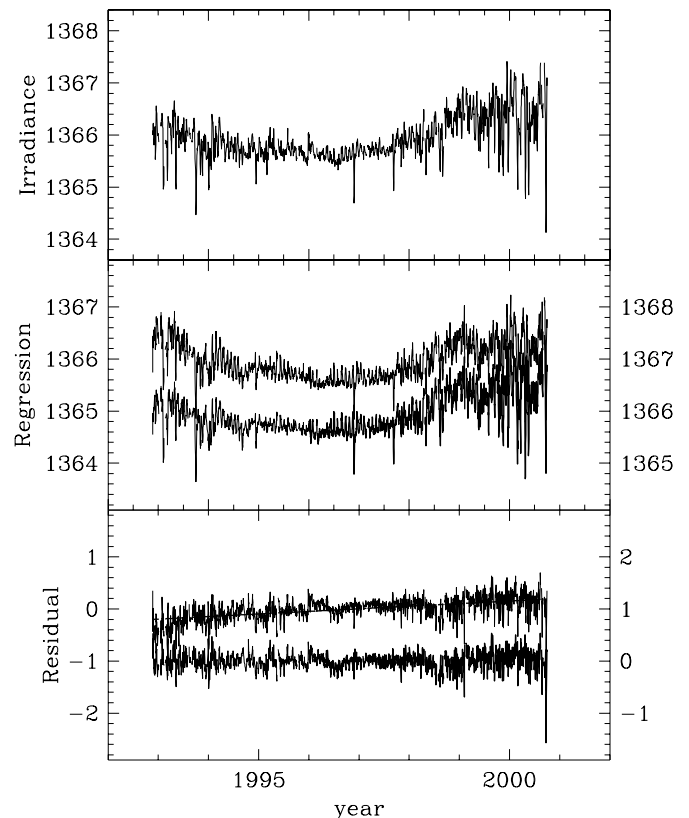


FIG. 4.—TSI (*top*), multiple regression fits (*middle*), and residuals (TSI–fits; *bottom*) as a function of time in units of years from 1992 November 21 to 2000 September 30. All abscissae are in units of W m^{-2} . The thick line in the upper curve of lower panel shows linear least-squares fit to the residuals for the entire period. The lower curves of middle and bottom panels show fits and residuals for regressions before (after) 1996 January 1, displaced by 1 W m^{-2} , as thin (thick) lines.

TSI variance in JBJW, while in this analysis the regressions are dominated by unipolar features.

It is worth noting that our regression analysis is purely correlative (indeed, all the basis variables, being normalized to zero mean and unit standard deviation, are dimensionless) and should not be considered physically predictive. This may partially account for the tendency of multiple R^2 in the above regressions to be somewhat lower than traditional analyses, particularly on rotational timescales and shorter. For example, although the division of the spatial domain into disk-center and limb domains is a coarse attempt to take into account the marked center-to-limb differences in facular contrast, we make no attempt to translate these contrasts to physical units by multiplying them by a standard limb-darkening curve. (In fact, it is not clear how to transform contrasts in equivalent width and line depth to physically relate to TSI variability.) Thus we are less likely to model accurately the passage of faculae across the visible disk.

A new feature appears in the current regression analysis for the total time period, which can be seen both in the bottom row of Table 3 and in the bottom panel of Figure 4. In addition to noise on short timescales (days–weeks), the plot shows systematic linear variation with a slope of about $0.05 \text{ W m}^{-2} \text{ yr}^{-1}$. The fit accounts for 30% of the variance in the residual curve, i.e., about 7% of the TSI variance, suggesting that if this trend were removed from the TSI data, multiple R^2 would increase to about 0.83. Over an 8 yr period this trend is a significant fraction of the TSI variation from solar minimum to maximum. One can also see from Table 3 and Figure 4 that there are no significant residual trends if the fit is segmented at 1996 January 1. However, the regression coefficients of the dominant factors for the two time periods differ from each other well beyond their formal errors in the sense that the composite TSI after 1996 January 1 depends more strongly on factor 1 (faculae) and less strongly on factor 2 (sunspots). As discussed below and in agreement with de Toma et al. (2001), these results imply either that there are systematic observational errors in one or both the TSI or SPM data sets or that an additional solar source of irradiance variation exists that is not detected in the SPM data.

5. DISCUSSION

The two major conclusions of JBJW are shown to extend to a decadal timescale. First, unipolar magnetic areas associated with active-region and active-network faculae and sunspots dominate the correlation of SPM observations with TSI. Second, strong-field, mixed-polarity regions (quiet network), although contributing substantially to the total variance of the SPM record, are effectively uncorrelated with TSI. The duration of our observations is not extensive enough to exclude quiet network as an important long-term source of solar irradiance variations. However, our data do span most phases of the sunspot cycle, and the correlation of TSI with mixed-polarity network is low enough to imply that any such contribution is likely to occur only on temporal scales considerably exceeding a solar cycle. Our analysis does not provide further insight into why TSI is poorly correlated with mixed-polarity network. We note that Jones (1998) was unable to find any indications of thermodynamic differences between unipolar and mixed-polarity regions with comparable LOS fluxes and speculate, as did JBJW, that quiet network is associated

with a “magnetic carpet” (Title & Schrijver 1998), which disappears and renews over times much shorter than a solar rotation period.

The linear temporal trend in the residuals of the multiple regression over the entire interval spanned by our data is consistent with a nonmagnetic solar source of TSI variation or with long-term, systematic, instrumental effects. We are unaware of any likely source of long-term instrumental trends in the SPM measurements of LOS field but plan to check on this possibility by comparing SPM observations with other measurements. Even if such a trend were found, however, we note that magnetic flux enters into our analysis only through the division of histograms into features and is not otherwise used in determining the measures that comprise the basis set for the factor analysis and multiple regression. Thus, a change in SPM sensitivity over time would modify the temporal variation of each factor but, to the extent that our representation is complete, would not affect the overall regression. There may, of course, be irradiance changes associated with magnetic features below the sensitivity or resolution limits of the SPM that would be undetected in our measurements.

In any case, a trend produced by a continuous phenomenon, such as might be expected from the changing sensitivity of a single instrument or a long-term solar variation, should be observed in regressions of subsamples of the data. However, evidence for long-term systematic variation of the residuals in the segmented regressions is absent, which suggests that the trend for the entire time period may be an artifact of forcing a continuous fit to disjoint intervals. Although the fit for either interval would be consistent with the two-component activity model of TSI variation, the dominant regression parameters for cycles 22 and 23 are distinctly different. It is possible to construct scenarios for which the response of actual TSI to solar activity, as measured by SPM, is different in cycle 23 than it was in cycle 22. For example, W. Livingston (2002, private communication) finds that sunspot umbrae in the $1.6 \mu\text{m}$ lines near the maximum of cycle 23 show weaker magnetic fields and intensity contrasts than do those drawn from a comparable sample during the maximum of cycle 22. These differences might be undetected in SPM measurements because of substantial photospheric stray light and would appear as a weaker sensitivity of TSI to observed sunspot properties in cycle 23. Unfortunately, it is not possible to test this idea directly since the SPM was not operational during the maximum of cycle 22. Similarly, if, in cycle 23, unipolar network and faculae were brighter in the UV for given photospheric properties, then an enhanced apparent response of TSI would be observed. Such a scenario would be consistent with the work of Unruh, Solanki, & Fligge (1999) and Preminger et al. (2002), who suggest that lines are responsible for the bulk of the cyclic variability of TSI as well as with observations of the Mg II h and k resonance lines, which tend to show comparable levels of emission in cycles 22 and 23. However, a source of chromospheric heating that is independent of photospheric magnetic properties detectable by the SPM would be required.

A simpler and perhaps more likely explanation involves uncompensated systematic instrumental effects. While there are no documented changes in SPM instrumentation or sensitivity between cycles 22 and 23, the observed composite TSI is sensitive to changes in the ensemble of operational radiometers, and one such change occurred on 1996

January 18 with the onset of VIRGO observations. Thus, the composite TSI, even though it has been carefully prepared to compensate for individual instrument sensitivities, plausibly records TSI with a different “gain” in cycle 23 than in cycle 22. Note that the SPM data fit the cycle 23 (predominantly VIRGO) observations best. Moreover, other composite records of TSI have been proposed. In particular, Willson (1997), using different assumptions about degradation of individual spacecraft radiometers, suggests that the value of TSI at solar minimum has not been constant over the past two solar cycles but has increased by about 0.036% per decade, which agrees well with the $0.05 \text{ W m}^{-2} \text{ yr}^{-1}$ trend (0.037% per decade) of our regression for 1992–2000. We plan to compare our results with Willson’s composite record of TSI in the near future.

6. FUTURE WORK

Our histogram-based technique tends to account for less TSI variance than the best representations based on other ground-based data, particularly in cycle 22. To understand better what aspects of our analysis lead to this result, we plan to compare the spatial structures that represent the factor patterns outlined in § 4.1 with other methods of feature classification, particularly those developed by Harvey & White (1999), Turmon, Pap, & Mukhtar (2002), and Preminger et al. (2001). The work of Turmon et al. (2002) in particular may suggest better posed multidimensional alternatives to our histogram classification. Functional relationships between all the SPM observables derived from histogram analysis can be cross-checked with predictions from extant models such as those constructed by Fontenla et al. (1999), Solanki & Unruh (1998), Fligge et al. (1998), and Unruh et al. (1999) to explore physical differences between features.

We have not attempted to separate quantitatively rotational, decadal, and other possible temporal scales in the

representation of either TSI or SPM data. However, we plan to apply singular spectrum analysis (Pap & Varadi 1996) and possibly other techniques, such as wavelet analysis, in the near future. This may help us understand what parts of the unexplained variance are attributable to different scales of variation and to clarify the lack of correlation between mixed-polarity features and TSI.

Finally, longevity and continuity are essential ingredients for any observational study of solar irradiance. Within calendar year 2003, the SPM will be retired from service to be replaced by the Vector Spectromagnetograph (VSM), a part of NSO’s Synoptic Optical Long-term Investigations of the Sun (SOLIS) instrumental package. The VSM will continue the observational repertoire of the SPM, albeit using a different spectral line, and will provide hitherto unavailable information regarding the vector magnetic field over the entire solar disk. Thus, important parts of our future work will be to complete analysis for the SPM data set, to ensure that the transition between the two instruments produces minimal discontinuity in the synoptic magnetogram record, and to develop methods for including the more complete physical description of the solar atmosphere provided by the VSM into our irradiance analysis.

The authors acknowledge useful discussions with G. Chapman, K. Harvey, W. Livingston, J. Pap, M. Turmon, and S. Walton as well as use of computer facilities at the University of Arizona for carrying out the factor and multiple regression analyses. The authors also wish to thank an anonymous referee for a very careful reading of the original manuscript and constructive comments that led to substantial improvements. This research was partially supported by NASA Supporting Research and Technology tasks 344-12-52-14 and 344-12-52-19. NSO/KPVT data used here were produced cooperatively by AURA/NSO, NASA/GSFC, and NOAA/SEC.

REFERENCES

- Chapman, G. A., Cookson, A. M., & Dobias, J. J. 1996, *J. Geophys. Res.*, 101, 13,541
- de Toma, G., White, O. R., Chapman, G. A., Walton, S. R., Preminger, D. G., Cookson, A. M., & Harvey, K. L. 2001, *ApJ*, 549, L131
- Fligge, M., Solanki, S. K., & Unruh, Y. C. 2000, *A&A*, 353, 380
- Fligge, M., Solanki, S. K., Unruh, Y. C., Fröhlich, C., & Wehrli, Ch. 1998, *A&A*, 335, 709
- Fontenla, J., White, O. R., Fox, P. A., Avrett, E. H., & Kurucz, R. L. 1999, *ApJ*, 518, 480
- Foukal, P., & Lean, J. 1988, *ApJ*, 328, 347
- Fröhlich, C. 2000, *Space Sci. Rev.*, 94, 15
- Fröhlich, C., & Lean, J. 1998, *Geophys. Res. Lett.*, 25, 4377
- Harman, H. H. 1976, *Modern Factor Analysis* (Chicago: Univ. Chicago Press)
- Harvey, K. L., & White, O. R. 1999, *ApJ*, 515, 812
- Jones, H. P. 1998, in *ASP Conf. Ser.* 140, *Synoptic Solar Physics*, ed. K. S. Balasubramaniam, J. W. Harvey, & D. M. Rabin (San Francisco: ASP), 145
- Jones, H. P., Branston, D. D., Jones, P. B., & Wills-Davey, M. J. 2000, *ApJ*, 529, 1070 (JBIW)
- Pap, J. M., & Fröhlich, C. 1998, *J. Atmos. Sol.-Terr. Phys.* 61, 15
- Pap, J. M., & Varadi, F. 1996, in *ASP Conf. Ser.* 95, *Solar Drivers of Interplanetary and Terrestrial Disturbances*, ed. K. S. Balasubramaniam, S. L. Keil, & R. N. Smartt (San Francisco: ASP), 576
- Preminger, D. G., Walton, S. R., & Chapman, G. A. 2001, *Sol. Phys.*, 202, 53
- 2002, *J. Geophys. Res.*, 107 (All), 10.1029/2001JA009169
- Solanki, S. K., & Unruh, Y. C. 1998, *A&A*, 329, 747
- Title, A. M., & Schrijver, C. J. 1998, in *ASP Conf. Ser.* 154, *10th Cambridge Workshop: Cool Stars, Stellar Systems, and the Sun*, ed. R. A. Donahue & J. A. Bookbinder (San Francisco: ASP), 345
- Turmon, M., Pap, J. M., & Mukhtar, S. 2002, *ApJ*, 568, 396
- Unruh, Y. C., Solanki, S. K., & Fligge, M. 1999, *A&A*, 345, 635
- Willson, R. C. 1997, *Science* 277, 1963